Conformational Plasticity of the Lipid Transfer Protein SCP2[†]

Fabian V. Filipp[‡,▽] and Michael Sattler*[,‡,§]

European Molecular Biology Laboratory, Meyerhofstrasse 1, D-69117 Heidelberg, Germany, GSF-National Research Center for Environment and Health, Ingolstädter Landstrasse 1, 85764 Neuherberg, Germany, and Technische Universität München, Lichtenbergstrasse 4, 85747 Garching, Germany

Received December 13, 2006; Revised Manuscript Received April 25, 2007

ABSTRACT: The nonspecific lipid transfer protein sterol carrier protein 2 (SCP2) is involved in organellar fatty acid metabolism. A hydrophobic cavity in the structure of SCP2 accommodates a wide variety of apolar ligands such as cholesterol derivatives or fatty acyl-coenzyme A (CoA) conjugates. The properties of this nonspecific lipid binding pocket are explored using NMR chemical shift perturbations, paramagnetic relaxation enhancement, amide hydrogen exchange, and ^{15}N relaxation measurements. A common binding cavity shared by different physiological ligands is identified. NMR relaxation measurements reveal that residues in the three C-terminal α-helices within the lipid binding region exhibit mobility at fast (picosecond to nanosecond) and slow (microsecond to millisecond) time scales. Ligand binding is associated with a considerable loss of peptide backbone mobility. The observed conformational dynamics in SCP2 may play a role for the access of hydrophobic ligands to an occluded binding pocket. The C-terminal peroxisomal targeting signal of SCP2 is specifically recognized by the Pex5p receptor protein, which conducts cargo proteins toward the peroxisomal organelle. Neither the C-terminal targeting signal nor the N-terminal precursor sequence interferes with lipid binding by SCP2. The α-helices involved in lipid binding also mediate a secondary interaction interface with the Pex5p receptor. Silencing of conformational dynamics of the peptide backbone in these helices upon either lipid or Pex5p binding might communicate the loading state of the cargo protein to the targeting receptor.

Lipid transfer proteins are auxiliary shuttles ensuring the appropriate localization of lipids in cellular subcompartments. Sterol carrier protein 2 (SCP2[1]) has been reported to interact with a wide variety of lipids associated with peroxisomal metabolism, including acyl-CoA conjugates as high-affinity ligands (*1*−*3*). Disruption of the *scp2* gene in mice suggests bile acids (soluble derivatives of cholesterol) and branched-chain fatty acid CoAs as physiological ligands to be functionally associated with SCP2 (*4*−*6*). Enzymes involved in both cholesterol secretion and fatty acid oxidation include the peroxisomal thiolase, acyl-CoA hydrogenase, and enoyl-CoA hydratase (*7*, *8*), all of which are expressed as fusion proteins with a sterol carrier protein domain fold (*9*). The transfer of fatty acyl-CoA substrates by SCP2 may have evolved to assist enzymes involved in branched chain fatty acid α-oxidation or very long chain fatty acid β-oxidation in the peroxisome (*8*). In this context SCP2 may play a role in substrate and/or product binding during peroxisomal bile acid synthesis and fatty acid oxidation.

Some molecular insight into the ligand binding site of the sterol carrier protein fold has been obtained from structural high-resolution studies of SCP2 bound to lipophilic molecules, i.e., a detergent (crystal structure bound to Triton X-100) (*10*), a fatty acid (crystal structure bound to palmitate) (*11*), or a spin-labeled fatty acid derivative (NMR structure and binding study with doxyl stearate) (*12*) (Figure 1). The binding pocket is formed by a central β-sheet, which is framed by α-helices creating a large cavity (Figure 1A) (*13*). The lipophilic ligands are deeply buried in this hydrophobic cavity of the protein. However, the ligands are located at different regions of the cavity and bind in opposite orientations with respect to their polar headgroups (Figure 1B,C). This presumably reflects the nonspecific lipid binding properties of SCP2.

Although the available three-dimensional structures of SCP2 orthologues free and when bound to ligands show a common tertiary fold, some structural differences are observed. While the β-sheet of the sterol carrier fold is well preserved, differences are observed for the lengths and orientations of the α-helices (Figure 1A−C). The structural variations observed in the molecular recognition of ligands by SCP2 suggest that the binding region may exhibit some conformational flexibility that would help to accommodate diverse lipophilic ligands. Dynamics could play a role for how the occluded binding cavity can be accessed by the lipophilic ligands. So far, an exper-

[†] This work was funded by the Deutsche Forschungsgemeinschaft and EMBL.

* Corresponding author. Telephone: +49-6221-387-552. Fax: +49-6221-387-98552. E-mail: sattler@embl.de.

[‡] European Molecular Biology Laboratory.

[§] GSF-National Research Center for Environment and Health and Technische Universität München.

[▽] Present address: University of California, San Diego, Department of Chemistry and Biochemistry, 9500 Gilman Drive, La Jolla, CA 92093−0307, USA.

[1] Abbreviations: SCP2, sterol carrier protein 2; mSCP2, mature isoform of SCP2; preSCP2, precursor isoform of SCP2; PTS1, peroxisomal targeting signal 1; Pexp, peroxisomal import protein, peroxin; TPR, tetratrico peptide repeat; CoA, coenzyme A; SCoA, stearoyl-CoA; LCoA, linoleoyl-CoA; ChA, cholic acid; TChA, taurocholic acid; DSA, doxylstearic acid; PRE, paramagnetic relaxation enhancement; K_D, equilibrium dissociation constant; CMC, critical micellar concentration; HSQC, heteronuclear single-quantum coherence; CPMG, Carr−Purcell−Meiboom−Gill.

10.1021/bi6025616 CCC: $37.00 © 2007 American Chemical Society
Published on Web 06/13/2007

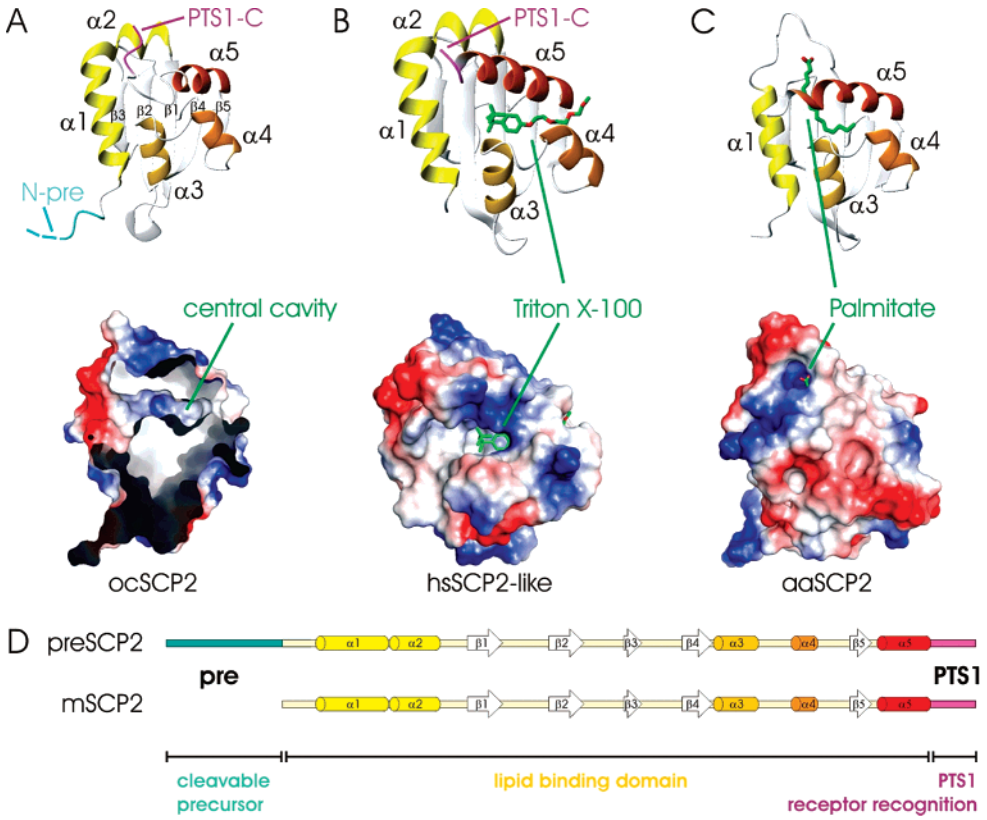

FIGURE 1: Structures of free SCP2 orthologues and when bound to lipophilic molecules. Secondary structure elements are annotated, and the C-terminal peroxisomal targeting signal 1 (PTS1) and the N-terminal precursor sequence (pre) are colored magenta and cyan, respectively. (A−C) Top panel: (A) Free mammalian SCP2 (oc, *Oryctolagus cuniculus*; PDB code 1C44) (*13*); (B) Triton X-100-bound human SCP2-like domain (hs, *Homo sapiens*; PDB code 1IKT) (*10*); (C) insect aaSCP2 in complex with bacterial palmitate (aa, *Aedes aegypti*; PDB code 1PZ4) (*11*). (A−C) Lower panel: (A) a surface representation of unliganded SCP2 (cut open) reveals a central hydrophobic cavity; (B) a Triton X-100 ligand is partially occluded; (C) a palmitate ligand is buried, leaving only the carboxyl terminus solvent-exposed. (D) Secondary structure and functional regions of SCP2. The precursor form of SCP2 (preSCP2) comprises at the N-terminus 20 amino acids in addition to the mature form (mSCP2).

imental characterization of conformational dynamics and its potential role in lipid binding by SCP2 is elusive.

The globular sterol carrier fold of SCP2 is flanked by flexible regions: an N-terminal precursor sequence and a C-terminal targeting signal (Figure 1D) (*12*, *14*). Targeting of SCP2 into the peroxisomal organelle depends on the recognition of its C-terminal peroxisomal targeting signal 1 (PTS1) by the cytosolic receptor protein Pex5p. The TPR domain of Pex5p specifically recognizes the basic and hydrophobic PTS1 sequence at the carboxy termini of proteins (*15*), corresponding to A141, K142, and L143 in SCP2. The SCP2−Pex5p cargo-receptor complex is tethered to the peroxisomal membrane and subsequently translocated into the peroxisomal matrix (*16*). Two isoforms of SCP2 can be detected in the cell, a precursor form (preSCP2) and a proteolytically cleaved, mature form (mSCP2), predominantly located in the cytosol (*9*). For both, the N-terminal 20 amino acid precursor sequence and the C-terminal PTS1 motif putative cellular functions have been proposed, such as in the modulation of lipid transfer or organellar sorting (*14*, *17*−*19*). The presence of a peroxisomal targeting signal and the involvement of SCP2 in organellar lipid homeostasis (*6*) suggest SCP2 as a model cargo protein for studying the peroxisomal import machinery (*20*).

Here, we characterize structural features and conformational dynamics of the free human SCP2 protein and when bound to various lipid ligands and to the TPR domain of the Pex5p receptor. We show that residues in the lipid binding site exhibit conformational dynamics at microsecond to millisecond time scales, which are silenced upon lipid binding. The potential interplay between flexible N- and C-terminal tails and lipid binding is investigated to probe their putative functional roles (*17*, *18*). We find no evidence for a previously proposed modulation of lipid binding by the C-terminal PTS1 motifs of SCP2. We show that a secondary binding interface between SCP2 and the Pex5p receptor partially overlaps with the α-helical lipid binding region. Conformational dynamics in this region is silenced upon lipid or Pex5p binding. This suggests a potential mechanism for how SCP2 may communicate the lipid loading state of SCP2 to Pex5p.

EXPERIMENTAL PROCEDURES

Protein Preparation. Precursor form preSCP2 (residues 1−143), mature form mSCP2 (residues 21−143), and the C-terminal TPR domain of human Pex5p (residues 315−639) (*20*) were expressed from a modified pET24d vector (Gunter Stier, EMBL Heidelberg) in *Escherichia coli* BL21-(DE3). The expressed proteins contained an N-terminal His_6-GST fusion, cleavable with tobacco etch virus (TEV) protease. Bacterial cultures were grown in LB medium or in M9 minimal medium supplemented with [U-^{13}C]-glucose and/or $^{15}NH_4Cl$ for the preparation of uniformly ^{13}C and/or ^{15}N isotopically labeled proteins. For the preparation of

deuterated proteins, cells were cultured in M9 minimal medium with ^2D_2O supplemented with $^{15}NH_4Cl$ and 1% ^2D,^{15}N-labeled growth medium (Silantes). Cell pellets were resuspended and lysed by sonication in the presence of protease inhibitors, and the lysate was cleared by centrifugation. The lysate was purified by affinity Ni-NTA agarose (QIAGEN). After an overnight incubation with His_6-tagged TEV protease (1 mg of protease/25 mg of protein) a second Ni-NTA agarose column removed uncleaved product, the His_6 tag, and the protease. The flow-through was subsequently subjected to gel filtration through a Superdex 75 (16/60) column (Pharmacia).

NMR Spectroscopy. NMR experiments were performed on 0.02−0.5 mM uniformly ^{13}C- and/or ^{15}N-labeled human preSCP2 and mSCP2 samples in the presence or absence of lipids or Pex5p receptor in 15 mM potassium phosphate, pH 6.0. NMR spectra were acquired on Bruker DRX500 and DRX800 spectrometers with cryogenic probes at 310 K unless stated otherwise. The backbone chemical shifts of preSCP2 and mSCP2 were based on BMRB entry 4438 (*12*) and extended using standard triple resonance experiments (*21*). Lipid derivatives (acid salts cholate, taurocholate, stearoyl-CoA, linoleoyl-CoA) were purchased from Sigma-Aldrich and dissolved in NMR buffer prior to NMR titration experiments. Chemical shift perturbations ($\Delta\delta = [(\Delta\delta^1H)^2 + (^1/_5\Delta\delta^{15}N)^2]^{1/2}$, in parts per million) were monitored in two-dimensional ^1H, ^{15}N correlation experiments. The potential presence of lipid micelles in the SCP2−lipid solutions was tested by dynamic light scattering (Supporting Information Figure 1). Solutions of SCP2 in the presence of lipids at concentrations below and above reported critical micellar concentrations [CMC(bile acids) > 0.8−10.0 mM) (*22*), CMC(acyl-CoAs) > 30−250 μM) (*23*)] show similar titration behavior (Supporting Information Figure 2).

Relaxation Analysis. Longitudinal (T_1) and transverse (T_2) ^{15}N relaxation and $\{^1H\}-^{15}N$ heteronuclear NOE experiments of free and lipid-bound SCP2 were recorded for backbone amides as described (*24*). Relaxation times were measured in an interleaved fashion with 12−14 relaxation delays for T_1 10.8−691.2 ms and T_2 (11.52−115.2 ms) at 295 K. The data were fitted to a single exponential decay with two parameters. Twice the noise level was used as an estimate of error, as suggested by repeated experiments. Dynamics at microsecond to millisecond time scales was analyzed by comparing intensity changes of the ^1H,^{15}N-HSQC reference experiment with an exchange-compensated experiment including 32 CPMG elements (*25*) at 290 K, 300 K, and 310 K. ^{15}N $T_{1\rho}$ relaxation data for SCP2 and SCP2−Pex5p were measured as described (*26*).

Paramagnetic Relaxation Enhancement Measurement with Spin-Labeled Lipids. Spin-label-induced paramagnetic relaxation enhancements were analyzed from intensity changes in ^1H,^{15}N-HSQC experiments of mSCP2 recorded in the presence of the fatty acid derivative 5-doxylstearic acid or 16-doxylstearic acid (Sigma-Aldrich) in the oxidized form and after reduction with ascorbic acid (*12*, *27*).

$^1H/^2D$ Exchange Experiments. $^1H/^2D$ exchange-protected amide protons were identified by recording ^1H,^{15}N-HSQC spectra with 512 and 32 complex points in t_2 and t_1, respectively, recorded with eight scans and an experimental time of 20 min on 0.5 mM SCP2 at 295 K at pH 6.0 after dissolving lyophilized samples in D_2O.

RESULTS

In order to characterize the unspecific lipid binding pocket, we titrated SCP2 with bile acids and acyl-CoA conjugates, representing two structurally quite diverse ligand classes of SCP2. The bile acid salts cholate (ChA) and taurocholate (TChA, conjugated at the side chain to the β-amino sulfonic acid taurin) are soluble sterol derivatives and were chosen for binding studies since they are important intermediates in cholesterol secretion (*4*, *7*) (Figure 2A). Stearoyl-CoA (18:0) (SCoA) is a long-chain saturated acyl-CoA, whereas linoleoyl-CoA (18:2) (LCoA) has two double bonds at C9 and C12 (Figure 2B). Both ligand classes bind to SCP2 with very different binding affinities. Determined by isothermal titration calorimetry the equilibrium dissociation constants for the interaction between SCP2 and SCoA are in the nanomolar to micromolar range (two binding sites, one high affinity, $K_D(1) = 89 \pm 30$ nM, $K_D(2) = 1.4 \pm 0.2$ μM; W. A. Stanley, S. Black, and C. Schultz, personal communication) (*2*, *28*). Compared to cholesterol (one binding site, $K_D = 4.2 \pm 0.7$ nM) (*28*), cholate shows reduced affinity in the micromolar range (one binding site, $K_D = 144 \pm 6$ μM) (Supporting Information Figure 3). Here, we characterize the ligand binding sites using chemical shift perturbations in NMR titrations and paramagnetic relaxation enhancements observed upon addition of spin-labeled ligands. The presence of conformational dynamics and the solvent accessibility of the binding pocket of SCP2 at different time scales are studied using ^{15}N relaxation measurements and $^1H/^2D$ exchange experiments in the absence and presence of ligands.

Chemical Shift Perturbation Mapping. NMR titration experiments of SCP2 with cholate and taurocholate (Figure 2A) affect amide protons in helices α1, α3, and α5 and sheets β1, β4, and β5 most strongly (Supporting Information Figure 4). Most of these residues are located in the C-terminal part of the SCP2 structure (Figure 2C; data shown for taurocholate). The chemical shift changes observed in the NMR titrations with acyl-CoAs (Figure 2B) are more widespread compared to the experiments with the bile acids and extend toward helices α1 and α2 (Figure 2C,D,F; Supporting Information Figure 4).

We next compared the NMR titrations of SCP2 with saturated and doubly unsaturated C18-acyl-CoA (SCoA and LCoA) (Figure 2B,D,E). The titrations of both acyl-CoAs are highly comparable (Figure 3). However, differences in the titration end points are observed in the C-terminal part of the SCP2 structure (Figure 3C,D). The residues that are differently affected suggest the location of the acyl chain of the ligands close to helices α3−α5 (Figure 2B,E). The nucleotide moiety of the acyl-CoA ligands cannot be directly localized, since no interaction of SCP2 to the very short chain acetyl-CoA is observed in NMR titrations, even at 100-fold molar excess.

Taken together, the NMR titration experiments for all ligands tested reveal strong chemical shift perturbations for a common set of residues in helices α3, α4, and α5 (Figure 2, Supporting Information Figure 4). The lipid binding site utilized by all four ligands tested overlaps well with the hydrophobic cavity (Figure 1A) and is consistent with the location of the phenyl moiety of Triton or C11−C16 of palmitic acid bound to SCP2 (Figure 1B,C) (*10*, *11*). This central binding cavity likely represents a high-affinity

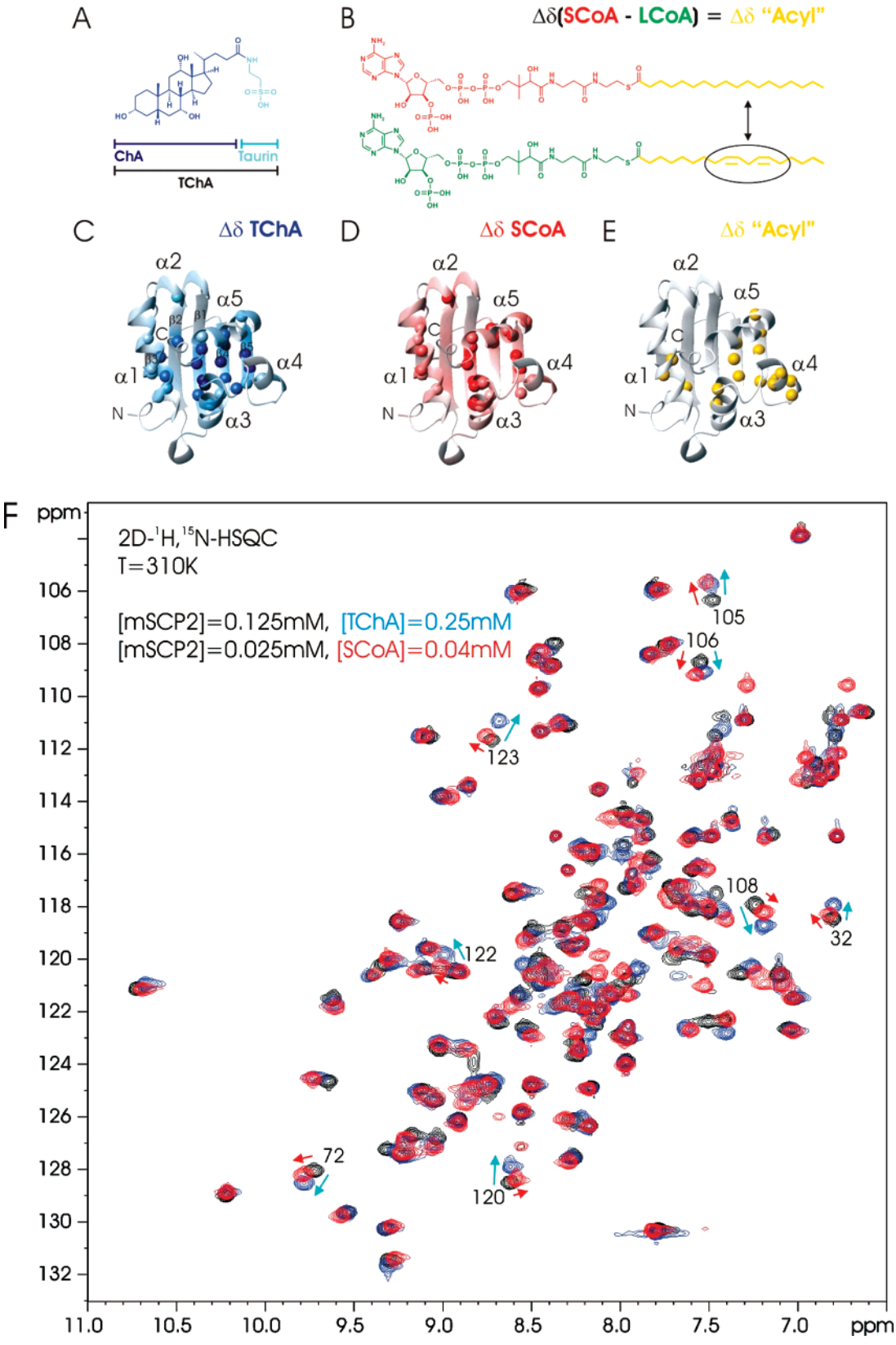

FIGURE 2: Chemical shift perturbations upon lipid binding to SCP2. NMR titration experiments of SCP2 with lipid ligands. (A) Taurocholic acid (TChA) is a conjugation of cholic acid (ChA) with the *β*-amino sulfonic acid taurin. (B) The binding of acyl-CoA conjugates is investigated for the saturated stearoyl-CoA (SCoA), the unsaturated linoleoyl-CoA (LCoA), and the acyl moiety. (C) The binding site of SCP2 is shown for the interaction with TChA. Strong chemical shift changes due to ligand binding ($\Delta\delta > 0.075$ ppm) are indicated by blue spheres onto a ribbon representation of mSCP2 (PDB code 1C44) (*12*). (D) Strong changes due to interaction of SCoA with SCP2 ($\Delta\delta > 0.075$ ppm) are indicated by red spheres. (E) Difference in binding between saturated and unsaturated acyl-CoA indicates the location of the acyl tail in the C-terminal part of the structure [$\Delta\delta$(acyl) = $\Delta\delta$(SCP2−LCoA) − $\Delta\delta$(SCP2−LCoA)] indicated in yellow. (F) Overlay of spectra of free SCP2 (black) and when bound to TChA (blue) or SCoA (red). Residues responding differently to the two ligand classes are labeled. The concentrations of protein (0.125 and 0.025 mM) and lipids (0.25 TChA and 0.04 mM SCoA) were chosen to obtain maximal saturation at lipid concentrations below the respective CMCs.

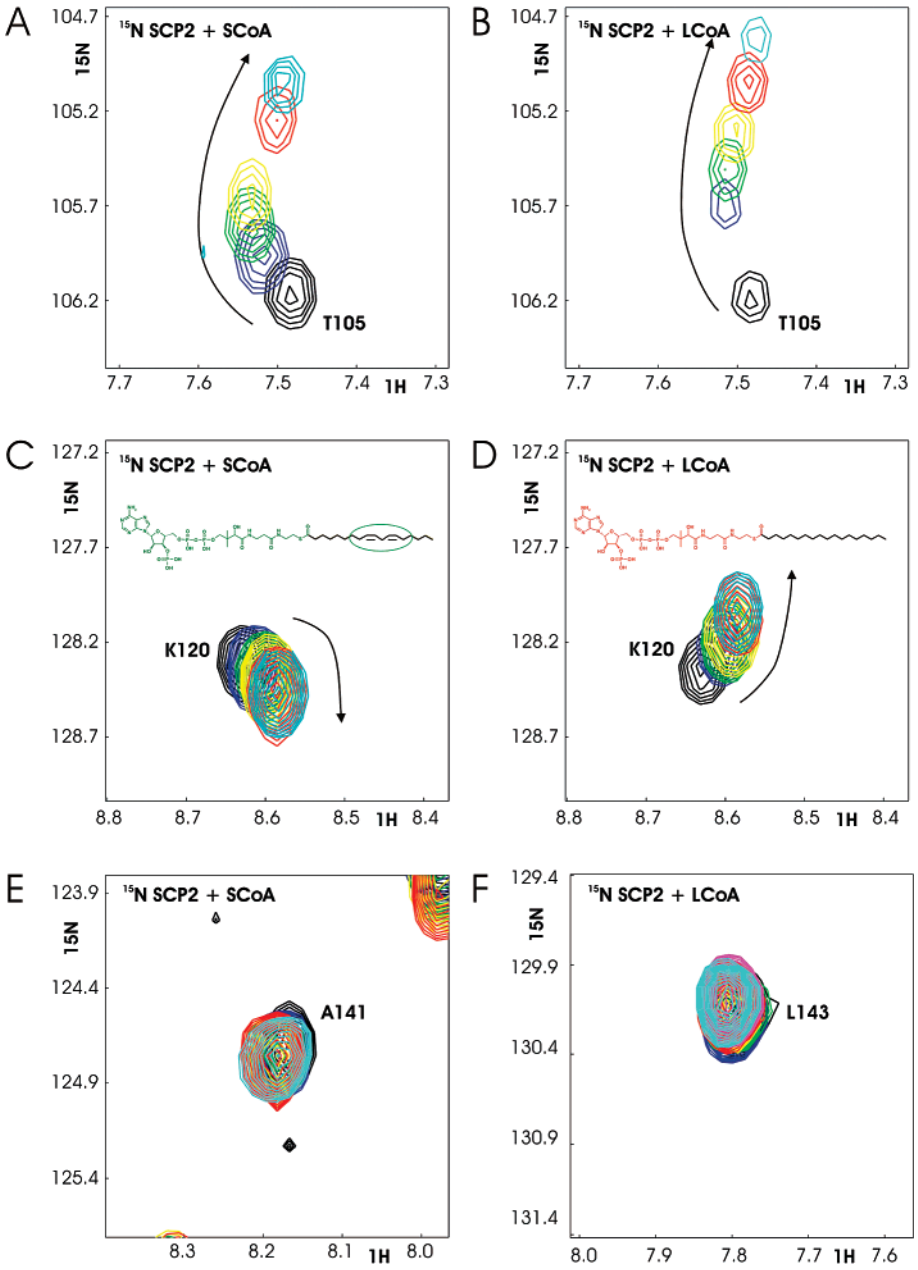

FIGURE 3: Chemical shift changes in NMR titrations of SCP2 with acyl-CoAs. Chemical shift changes observed in NMR titration experiments of SCP2 with stearoyl-CoA (SCoA) and linoleoyl-CoA (LCoA). (A−D) Residues within the lipid binding site exhibit strongly curved peak traces. (A, B) For most residues very similar chemical shift perturbations are observed for both acyl-CoA ligands. (C, D) However, amides of residues in α1 (T105) and α3−α5 (K120) respond differently to the saturated (SCoA) or doubly unsaturated (LCoA) acyl-CoA ligand. (E, F) Residues in the C-terminal PTS1 tail are not affected by the addition of lipid ligands. The protein concentration was 0.2 mM (free, black), and titration points were measured at protein:ligand molar ratios of 1:0.5 (blue), 1:0.8 (green), 1:1 (yellow), 1:2.4 (red), and 1:4 (cyan).

target site that has general binding affinity for hydrophobic ligands (*28*).

Paramagnetic Relaxation Enhancements. Chemical shift perturbations do not only indicate changes due to direct intermolecular protein−ligand contacts but also report on indirect changes of structure and/or conformational dynamics in response to the ligand burial. Therefore, we employed an alternative experimental approach to more directly map the ligand binding site using paramagnetic relaxation enhancement (PRE) experiments (*27*) with spin-labeled acyl derivative ligands (Supporting Information Figure 5). The binding of 5-doxyl- or 16-doxylstearic acid shows a bleaching pattern that mainly affects residues in helices α1 and α3−α5, with smaller effects for residues in the β-sheet. Thus, the PRE data and the chemical shift perturbation data confirm the hydrophobic cavity in SCP2 as the lipid binding site, which most likely accommodates the acyl moiety of acyl-CoAs and stearic acid derivatives studied (Figure 2, Supporting Information Figures 4 and 5).

^{1}H/^{2}D Exchange Experiments. A footprint of the ligand on the protein structure can be monitored in ^{1}H/^{2}D exchange experiments recorded in the absence and presence of high-affinity ligands (*29*). In the absence of ligands, we observe protected amide groups in all secondary structure elements of the SCP2 core structure with the exception of helices α4 and α5. No amides are protected in the N-terminal precursor or the C-terminal PTS1 tails of SCP2. In the presence of lipid ligands, the ^{1}H/^{2}D exchange experiments show ad-

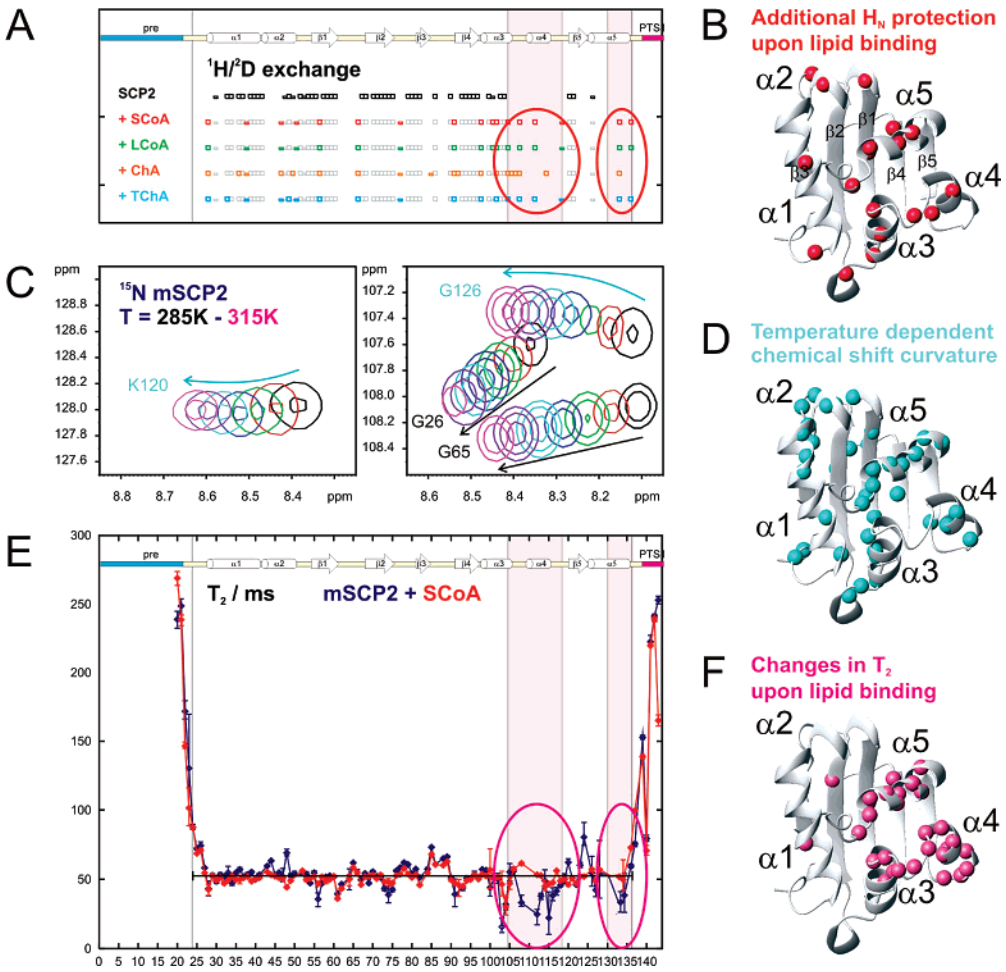

FIGURE 4: ^{1}H/^{2}D exchange experiments, temperature dependence of chemical shifts, and ^{15}N T_2 relaxation data of SCP2 (free and bound to lipid ligand). (A) ^{1}H/^{2}D exchange experiments of m- and preSCP2 at 0.125 mM at 295 K. Protected amides are indicated by the presence of the amide proton NMR signal after 10 min. The pattern of protected amides is comparable for both forms of SCP2; no protected amides could be detected in the N-terminal precursor, helices α4 and α5, and the C-terminal peroxisomal targeting signal. In the presence of lipid ligands, stearoyl-CoA (SCoA, 0.4 mM, red), linoleoyl-CoA (LCoA, 0.4 mM, green), cholate (ChA, 1.0 mM, orange), and taurocholate (TChA, 1.0 mM, cyan), additional amides become protected. (B) This is indicated by spheres if the protection effect is observed for at least three different ligands. (C) Spectral regions showing chemical shift changes depending on the temperature of mSCP2 at 285 K (black) to 315 K (magenta) in steps of 5 K. The chemical shifts of residues G26 and G65 show a linear temperature dependence, whereas the chemical shifts of K120 and G126, for example, show a curve temperature dependence. (D) Residues with curved chemical shift temperature dependence are mapped onto the structure of SCP2, indicating regions involved in conformational exchange (*30*). (E) ^{15}N T_2 relaxation experiments show that the N- and C-termini are highly flexible independent of the absence or presence of lipid ligands. In the free state (0.4 mM mSCP2, blue), residues in the core of the SCP2 fold have an average T_2 value of 52 ms, consistent with a monomer of 13.4 kDa (^{15}N T_1/T_2 = 14 at 295 K). Residues in helices α4 and α5 have reduced T_2 values indicative of exchange broadening. This effect is lost in the presence of the stearoyl-CoA ligand (0.8 mM, red). (F) Residues with lower T_2 values in the absence of SCoA than in the presence of SCoA are highlighted on the structure of SCP2.

ditional protected amides compared to free SCP2 especially for residues in helices α3−α5 (Figure 4A,B). The additional protection may result from direct shielding of amides from the solvent and/or from rigidifying of the protein backbone associated with ligand binding. The region exhibiting additional protection of amides in the presence of lipid ligands agrees well with the chemical shift perturbation and PRE data (Figures 2C,D and 4B, Supporting Information Figure 5).

NMR Titration Curves. In the course of the NMR titrations of SCP2 with lipid ligands the traces of amide chemical shift changes are in many cases strongly curved (Figure 3, Supporting Information Figure 6). This demonstrates that the ligand binding event is more complex than a simple docking of two rigid bodies. Several possibilities may account for this: The curved titration traces may indicate the binding site of a second ligand (with weaker affinity), structural rearrangements linked with ligand binding, and/or a change in conformational dynamics upon ligand binding.

The existence of conformational flexibility is suggested by a significant temperature dependence of the amide chemical shifts. In rigid parts of the molecule increased random motion at elevated temperatures correlates with a linear change of chemical shifts, while regions of a protein involved in conformational exchange processes between alternative conformations will exhibit a curved temperature dependence of chemical shifts (*30*). In SCP2 significantly curved chemical shift temperature dependences are observed for 41 of 126 backbone amides including all α-helices in the structure (Figure 4C,D). The residues affected are located in the surrounding of the lipid binding cavity.

Conformational Dynamics at Microsecond to Millisecond Time Scales. The NMR titrations (as a function of lipid ligands and temperature) as well as the ^{1}H/^{2}D exchange

experiments suggest that ligand binding of SCP2 is associated with a reduction in backbone mobility of residues located in the binding site. We, therefore, wished to further characterize this potential conformational dynamics. First, we recorded ^{15}N relaxation data for SCP2 free and in complex with acyl-CoAs (Figure 4E,F, Supporting Information Figure 7). The relaxation data of the free and acyl-CoA-bound state show differences in the hetereonuclear NOE and transverse (T_2) relaxation values in the C-terminal region (residues 100−135, comprising helices α3−α5) of SCP2 (Supporting Information Figure 7). Differences in the heteronuclear NOE indicate that mobility at picosecond to nanosecond time scales is lost upon lipid binding. Residues in the three C-terminal helices also exhibit lower ^{15}N T_2 relaxation times in free SCP2 (compared to the average value). This suggests conformational mobility at slower (microsecond to millisecond) times scales for these residues. Notably, the reduced ^{15}N T_2 relaxation times are only observed in the unliganded state. Thus, the ^{15}N relaxation experiments indicate that peptide backbone mobility in this C-terminal region is reduced upon lipid binding.

We further examined mobility at microsecond to millisecond times scales by using exchange relaxation compensated HSQC experiments (*31*, *32*). The exchange contribution to transverse relaxation during the pulse sequence of a ^{1}H,^{15}N-HSQC experiment can be refocused using Carr−Purcell−Meiboom−Gill (CPMG) spin echoes (*25*, *33*). By reducing the exchange contribution to the relaxation process, an increased intensity ratio of HSQC to CPMG signals is observed for residues which exhibit dynamics on microsecond to millisecond time scales. The exchange contribution was studied at three different temperatures (290, 300, and 310 K) in the absence and presence of linoleoyl-CoA (Figure 5). At 310 K the majority of backbone residues in free SCP2 are not subject to chemical exchange processes at microsecond to millisecond time scales (Figure 5A). At lower temperatures amide signals of all helical secondary structure elements are strongly subject to broadening due to exchange (Figure 5B−D). The presence of the linoleoyl-CoA ligand silences these motions, and residues 100−136 are most strongly affected by this reduction in backbone mobility (Figure 5E). Remarkably, the region that experiences a strong reduction of dynamics correlates well with helices α3−α5 framing the ligand binding cavity of SCP2 (Figure 2). A more detailed and quantitative analysis can be obtained from relaxation dispersion experiments at different temperatures and different field strengths. Preliminary measurements confirm that binding site residues exhibit significant relaxation dispersion (data not shown).

Unstructured Precursor and Targeting Sequences Do Not Influence Ligand Binding. We have also studied the effect of the precursor and C-terminal PTS1 targeting sequences on the SCP2−lipid interaction (Figure 1). We compared binding of linoleoyl-CoA to the precursor form (preSCP2) and the mature form (mSCP2), lacking the N-terminal precursor sequence. Titration experiments of mSCP2 and preSCP2 with lipid ligands are highly comparable, and no differences in terms of binding affinity or the extent of chemical shift perturbation are observed (data not shown) (*26*). No chemical shift perturbations are observed for residues in the N- or C-terminal tails of mSCP2 upon lipid binding. The precursor sequence and the PTS1 motif exhibit low heteronuclear NOE values, shorter ^{15}N T_1 and longer ^{15}N T_2 relaxation times compared to the structured core of SCP2, and no solvent-protected amides could be detected for residues in the N- or C-terminal tail (Supporting Information Figure 7, Figure 4A). In addition, the intensities and positions of NMR signals of residues in the C-terminal PTS1 sequence are virtually identical in spectra of preSCP2 or mSCP2, indicating that there is no interaction between the N-terminal precursor sequence and the C-terminal PTS1 motif, consistent with previous findings (*14*). Thus, ^{1}H/^{2}D exchange experiments, line shape and relaxation analyses confirm that the two termini lack structural order in the absence or presence of lipid ligands.

Interaction with the Peroxisomal Targeting Receptor Pex5p. Peroxisomal import is proposed to translocate folded, liganded, and functional cargo proteins across the peroxisomal membrane (*34*). In order to assess whether the interaction of SCP2 with the peroxisomal targeting receptor Pex5p can modulate the lipid binding of SCP2, we have titrated SCP2 with lipid ligands in the absence and presence of the TPR domain of the Pex5p receptor (Figure 6, Supporting Information Figure 8). The formation of a stable 50 kDa SCP2−Pex5p cargo-receptor complex (free Pex5p, PDB code 1C0M; mSCP2-bound Pex5p, PBD code 1C0L) (*26*) is evidenced by large chemical shift changes in the C-terminal PTS1 of SCP2 (Figure 6A) and an overall reduction of ^{15}N transverse relaxation times (Figure 6D). When stearoyl-CoA is added to a complex of ^{15}N-labeled mSCP2 and the unlabeled Pex5p TPR domain, chemical shift perturbations are observed in the same regions as seen in the titration of mSCP2 without Pex5p, i.e., helices α1−α5 (Figure 6B,C, Supporting Information Figure 8); albeit absolute values of the chemical shift perturbations are decreased compared to binding of SCoA to SCP2 alone.

In addition to the interaction of the C-terminal PTS1 motif of SCP2, helices α1 and α3 form a secondary binding interface with the Pex5p receptor (*26*). The chemical shift perturbations upon lipid binding show that, even when bound to Pex5p, SCP2 can bind its lipid ligands and confirm experiments using spin-labeled lipid derivatives (*26*). However, the reduced size of the chemical shift perturbations supports that the binding site properties are modulated. A comparison of transverse ^{15}N ($T_{1\rho}$) relaxation times of SCP2 free and bound to Pex5p indicates that conformational dynamics on microsecond to millisecond time scales seen for helices α3−α5 in free SCP2 (Figures 5, 6D) is not present when bound to Pex5p (Figure 6D). Thus, conformational dynamics, which is present in free SCP2, is lost upon either binding to lipid ligands or binding to Pex5p. Intriguingly, helices α1 and α3 are part of the lipid binding site and also constitute the secondary binding interface with Pex5p (Figure 6E) (*26*).

DISCUSSION

Binding of Structurally Diverse Ligands into a Hydrophobic Binding Pocket. Our data show that the SCP2 protein can be divided into three functionally independent segments: a disordered N-terminal precursor motif due to alternative translation initiation, a core domain mediating lipid binding, and a structurally independent peroxisomal targeting signal responsible for protein sorting (Figure 1D).

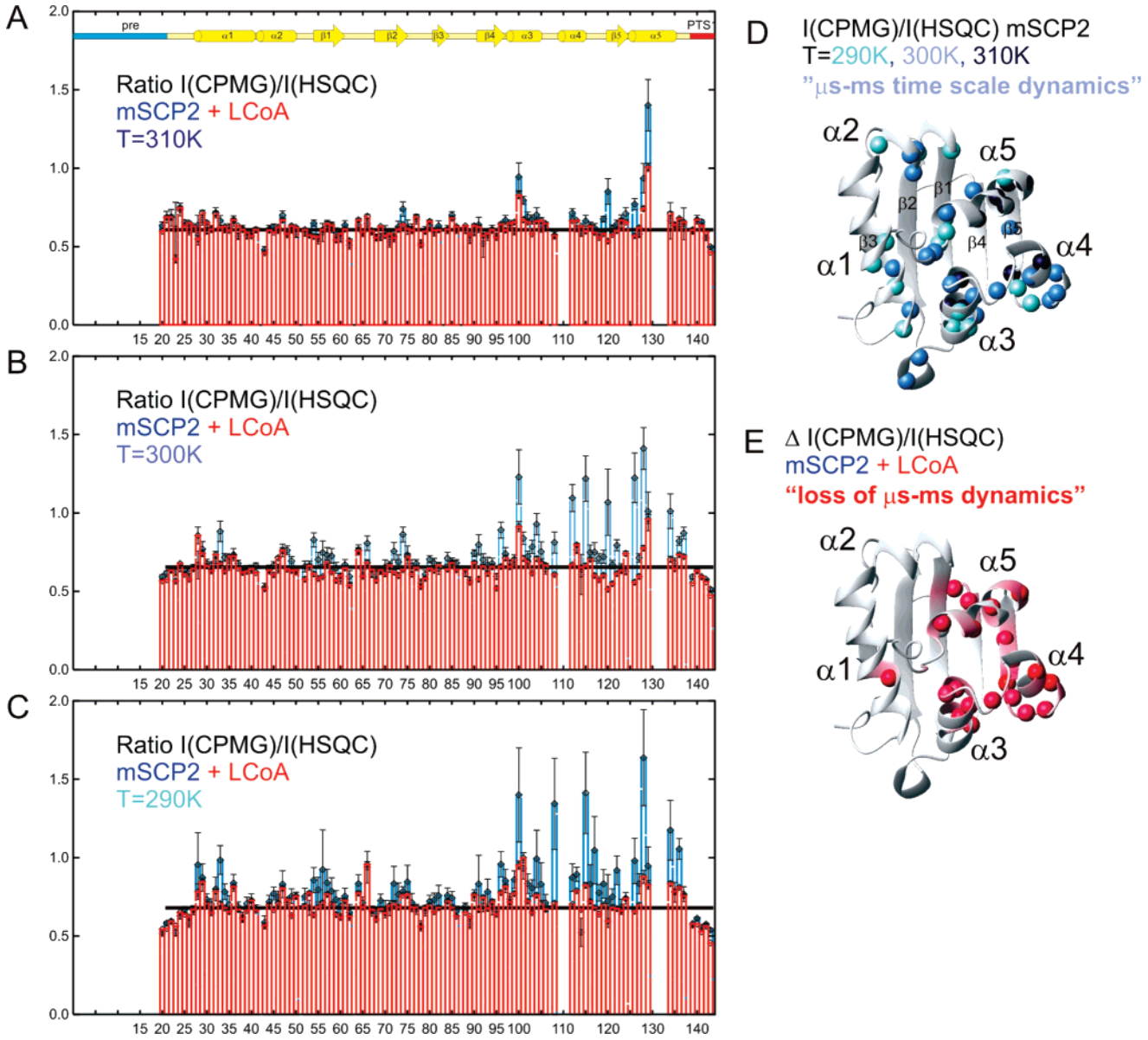

FIGURE 5: Conformational dynamics at microsecond to millisecond time scales in free and lipid-bound SCP2. (A−C) Intensity ratio of NMR signals in $^{1}H,^{15}N$-HSQC experiments of 0.2 mM mSCP2 with and without a 32 exchange relaxation compensating CPMG element during the pulse sequence recorded at 290 K, 300 K, and 310 K in the absence (blue) and presence of linoleoyl 0.4 mM LCoA (red). For most residues an average intensity ratio I(CPMG)/I(HSQC) of 0.63 ± 20% is observed. (D) Residues strongly affected (with a intensity ratio >0.75) are displayed as spheres on the structure of SCP2. (E) Residues whose intensity ratio is strongly affected by LCoA binding show reduced intensity ratios by more than 25% and are plotted onto the structure of SCP2.

We have studied the interaction of SCP2 with physiological ligands and confirmed that the hydrophobic cavity of SCP2 is a common binding site for lipophilic ligands. The chemical shift perturbation data suggest that helices α3−α5 mediate the binding of the acyl chain. Nonspecific hydrophobic interactions presumably dominate the interaction, which may explain the binding preference for acyl-CoA derivatives (K_D = 89 ± 30 nM; W. A. Stanley, personal communication), long-chain fatty acids (K_D = 234 ± 47 nM) (*35*), and cholesterol (K_D = 4.2 ± 0.7 nM) (*28*). Polar side chains lining the hydrophobic binding cavity might contribute additional electrostatic contacts and be responsible for the observed binding preferences for acyl-CoAs over more polar lipids such as bile acids. For example, polar modifications of the sterol scaffold of cholesterol substantially lower the affinity for bile acids (K_D = 144 ± 6 μM) (Supporting Information Figure 3) significantly compared to cholesterol.

The Conformation of Termini Is Independent of the Lipid Binding Domain. Both the N- and C-terminal precursor and PTS1 sequences are unstructured and highly flexible in pre/mSCP2. None of the residues in the 20 amino acid N-terminal precursor or the three C-terminal residues of the peroxisomal targeting signal are affected in the lipid titrations and remain flexibly disordered (data not shown). Further, the N-terminal precursor does not influence the interaction with the peroxisomal targeting receptor Pex5p (*26*). These data show that a previously proposed putative function of the N-terminal precursor motif for organellar sorting (*18*) is structurally clearly separated from the lipid binding function of the core domain.

Recently, it was described that removal of a lipophilic ligand in a molecular dynamics simulation caused the C-terminus to collapse into a coiled-coil conformation and the PTS1 residues to retract toward the protein, leaving them

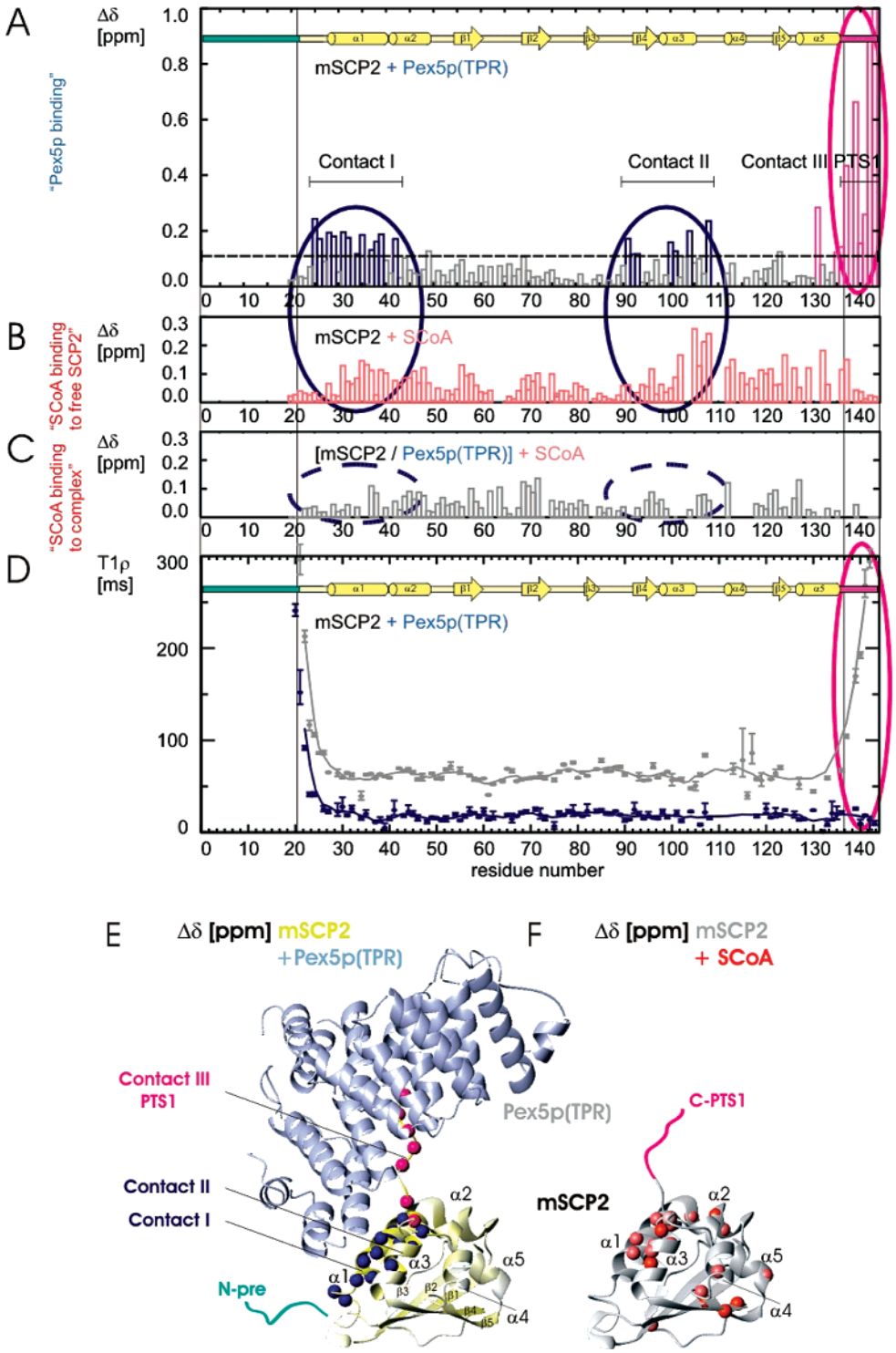

FIGURE 6: Effects of the peroxisomal import receptor Pex5p TPR domain on lipid binding of SCP2. (A) Chemical shift perturbations $\Delta\delta$ upon binding of the Pex5p TPR domain (0.2 mM) to ^{15}N mSCP (0.2 mM) affect two secondary binding regions (contacts I and II, blue) in addition to the major interaction site mediated by the C-terminal PTS1 (contact III, magenta). (B, C) Chemical shift perturbation upon binding of stearoyl-CoA to 0.4 mM ^{15}N mSCP2 in the absence (B) and in the presence (C) of the equimolar Pex5p TPR domain. (D) Comparison of ^{15}N ($T_{1\rho}$) transverse relaxation experiments of free mSCP2 and when bound to Pex5p TPR domain. The $T_{1\rho}$ values of flexible terminal regions are significantly higher compared to the average values for residues in the core of the domain. Due to the interaction with Pex5p, $T_{1\rho}$ values of residues in the PTS1 tail are strongly reduced, indicating that they become highly ordered. The large difference in molecular mass between free mSCP2 (13.4 kDa) and the SCP2/Pex5p TPR domain complex (49.6 kDa) is reflected in a general reduction of the average $T_{1\rho}$ values. (E) Strong chemical shift perturbations ($\Delta\delta > 0.075$ ppm) are plotted onto a ribbon representation of mSCP2 in complex with the Pex5p TPR domain (PDB code 1C0M) (*26*). Besides the main interaction site via the PTS1 (magenta), additional contacts are employed (contacts I and II, blue). (F) Lipid binding affects the secondary binding site of Pex5p but not the PTS1 tail (compare to Figure 2D).

poorly exposed (*17*). By reversing this observation, a ligand-assisted targeting mechanism was proposed, where the PTS1 motif is pushed away from the SCP2 fold in response to ligand binding, thereby exposing the PTS1 residue uptake for the interaction with the Pex5p receptor. However, at variance with this model none of our experiments indicate

that the PTS1 is affected by the presence of a lipid ligand (Figures 3E,F, 4E, and 6C, Supporting Information Figures 4, 6, and 7). The ^{15}N relaxation data clearly show that the targeting signal is disordered and highly flexible, independent of the core lipid binding domain or its ligand binding state. Thus, the proposed ligand-assisted targeting mechanism (*17*) is not supported by our data. The flexibility of the linker connecting the last α-helix of the sterol carrier fold and the PTS1 motif demonstrates that lipid binding and Pex5p binding by SCP2 are modular and structurally separated.

Conformational Dynamics of α*-Helices Framing the Lipid Binding Cavity.* SCP2 binds nonspecifically to various lipid ligands. This is also reflected by structural variations seen in the crystal structures of SCP2 bound to Triton X-100 or palmitate (*10*, *11*). The available free and ligand-bound SCP2 structures are very similar with respect to the central *β*-sheet (*11*, *12*) but deviate most in the layer of α-helices attached to the *β*-sheet scaffold (*10*−*13*) (Figure 1).

Here, we have shown that the structural plasticity seen in the free and ligand-bound structures of SCP2 is paralleled by conformational dynamics. The NMR titrations of SCP2 with bile acids and acyl-CoAs show a curved behavior (Figure 3) (*30*). The bent titration curves indicate that the backbone amides experience different chemical environments in the course of the titration, reflecting not only the degree of saturation of the ligand binding site but also associated conformational changes in the protein. Conformational dynamics is further indicated by the unusual amide chemical shift temperature dependence, which is curved for many residues located in the core binding cavity (Figure 4C,D). These data indicate that ligand binding by SCP2 is intimately linked with conformational dynamics.

Our NMR relaxation data (Figure 4E,F, Supporting Information Figure 7) provide direct evidence for the presence of conformational flexibility (at picosecond to nanosecond time scales) in the SCP2 peptide backbone, which is also hinted by elevated X-ray *B*-factors in the C-terminal part of the SCP2 structures (*10*, *13*). Moreover, the CPMG/HSQC experiments (Figure 5) indicate the presence of backbone dynamics also at slow (microsecond to millisecond) time scales. The NMR relaxation experiments show that helices α3−α5 are strongly involved in these dynamic processes. Intriguingly, the mobility of helices α3−α5 seen in the relaxation data is lost in the presence of lipid ligands. This correlates well with the additional protection of amide protons observed for the same region in ^{1}H/^{2}D exchange experiments (Figure 4A,B).

The ability of this region of the protein to adapt its conformation in response to ligand interaction is very likely linked to the nonspecific lipid binding properties of SCP2. Conformational dynamics may enable structurally quite diverse lipid ligands to access the occluded hydrophobic cavity and to optimize protein−ligand contacts as seen in the structural plasticity of the SCP2−ligand complexes. A related model has been proposed for the cavity mutant L99A of lysozyme, where residues framing the hydrophobic cavity sample a higher energy state (*36*) and exchange processes facilitate the rapid uptake of hydrophobic ligands into an otherwise inaccessible binding pocket.

Other lipid binding protein classes also exhibit plasticity and dynamics in their ligand binding pocket. The crystal structure of the liver bile acid-binding protein shows structural plasticity that enables the protein to bind two molecules of cholic acid (*37*). The proposed entry portal of adipocyte fatty acid-binding protein displays a high degree of flexibility evidenced by ^{15}N and ^{2}H relaxation analysis (*38*). Conformational dynamics of the ligand entry site may allow the protein to bind larger ligands in comparison with fatty acid-binding proteins with more rigid binding cavities.

In addition to mobility of residues in the lipid binding region of the protein, fatty acid ligands themselves might not be rigidly anchored within the binding pocket (*39*). A NMR relaxation study of myristate bound to human serum albumin has revealed that the lipid is mobile within its limited binding cavity (*40*). The widespread chemical shift perturbations affecting many amides during the lipid titrations with SCP2 could therefore, in addition to changes in protein dynamics, also reflect mobility of the lipid ligand within the hydrophobic cavity.

Potential Cross-Talk between Lipid Binding and Pex5p Binding. The equilibrium binding constants for the interaction of SCP2 free and when bound to Pex5p with lipid ligands are very similar [K_D(Pex5p + mSCP) = 109 ± 34 nM, K_D(Pex5p + mSCP(SCoA) = 124 ± 17 nM (*26*)], suggesting that lipid binding is independent of the Pex5p interaction. Nevertheless, the observed reduction in conformational dynamics in the C-terminal region of SCP2 upon binding to lipids or to Pex5p could represent a mechanism for how the receptor may sense the lipid loading state of its cargo protein (i.e., SCP2). The Pex5p peroxisomal targeting receptor contacts SCP2 via a secondary binding site, which intriguingly overlaps with regions involved in lipid binding (Figure 6E). The NMR relaxation data show that conformational dynamics of residues located in this region site is lost upon binding of SCP2 to either the lipid ligand or the Pex5p receptor (Figures 4E, 6D). Thus, the binding of SCP2 to lipids causes the binding region to rigidify. Therefore, the binding of lipid-loaded SCP2 may be associated with a smaller loss in conformational entropy upon binding to the Pex5p receptor. As the equilibrium lipid binding affinities of SCP2 and SCP2-Pex5p are very similar, this effect must be small at least under equilibrium conditions. However, the binding kinetics could be altered and communicate the lipid loading state nevertheless: The silencing of conformational dynamics in the lipid binding site upon Pex5p binding could play a role in preserving the lipid loading state of SCP2 while bound to the targeting receptor. Peroxisomal protein import is proposed to involve translocation of folded substrates (*34*) and thus requires passing through a lipophilic membrane. In this environment, the SCP2−lipid complex might disassemble during the import process and the lipid could escape into the membrane, instead of being transferred to the peroxisomal matrix. A rigidified import complex may thus support the lipid transfer activity of SCP2 during peroxisomal protein import via Pex5p.

Numerous cellular functions have been proposed for SCP2, and previous structural and biochemical studies have contributed to understanding the protein as a cargo for organellar import. Here, we show that the ability of SCP2 to bind to structurally quite diverse ligands may be intimately linked to conformational dynamics on microsecond to millisecond time scales. A reduction of this mobility upon ligand binding might communicate the lipid loading state of SCP2 to the peroxisomal targeting receptor and play a role for translo-

cation across the membrane. These functional properties enable the unspecific lipid binding protein SCP2 to be effectively involved in organellar lipid transfer and maintenance of lipid homeostasis.

ACKNOWLEDGMENT

We thank Will Stanley (EMBL Hamburg) for stimulating discussions and Bernd Simon (EMBL Heidelberg), Vladimir Rybin (EMBL Heidelberg), and Phineus Markwick (IBS Grenoble) for support with data acquisition and analysis.

SUPPORTING INFORMATION AVAILABLE

Figure 1, Dynamic light scattering of SCP2−lipid solutions; Figure 2, NMR spectra of SCP2 and SCP2−lipid complexes below and above the critical micellar concentration of linoleoyl-CoA; Figure 3, Isothermal titration calorimetry data for cholate binding to SCP2; Figure 4, Summary of NMR chemical shift perturbations for SCP2 with various lipid ligands; Figure 5, Paramagnetic relaxation enhancements (PRE) for binding of spin-labeled lipid derivatives to SCP2; Figure 6, Chemical shift changes in NMR titrations of SCP2 with bile acids; Figure 7, NMR ^{15}N relaxation data for SCP2 isoforms free and when bound to lineoyl-CoA; Figure 8, NMR spectra of SCP2 free and when bound to Pex5p in the absence and presence of stearoyl-CoA. This material is available free of charge via the Internet at http://pubs.acs.org.

REFERENCES

1. Dansen, T. B., Westerman, J., Wouters, F. S., Wanders, R. J., van Hoek, A., Gadella, T. W., Jr., and Wirtz, K. W. (1999) High-affinity binding of very-long-chain fatty acyl-CoA esters to the peroxisomal non-specific lipid-transfer protein (sterol carrier protein-2), *Biochem. J. 339* (Part 1), 193−199.
2. Frolov, A., Cho, T. H., Billheimer, J. T., and Schroeder, F. (1996) Sterol carrier protein-2, a new fatty acyl coenzyme A-binding protein, *J. Biol. Chem. 271*, 31878−31884.
3. Gallegos, A. M., Atshaves, B. P., Storey, S. M., Starodub, O., Petrescu, A. D., Huang, H., McIntosh, A. L., Martin, G. G., Chao, H., Kier, A. B., and Schroeder, F. (2001) Gene structure, intracellular localization, and functional roles of sterol carrier protein-2, *Prog. Lipid Res. 40*, 498−563.
4. Fuchs, M., Hafer, A., Munch, C., Kannenberg, F., Teichmann, S., Scheibner, J., Stange, E. F., and Seedorf, U. (2001) Disruption of the sterol carrier protein 2 gene in mice impairs biliary lipid and hepatic cholesterol metabolism, *J. Biol. Chem. 276*, 48058−48065.
5. Noland, B. J., Arebalo, R. E., Hansbury, E., and Scallen, T. J. (1980) Purification and properties of sterol carrier protein2, *J. Biol. Chem. 255*, 4282−4289.
6. Seedorf, U., Raabe, M., Ellinghaus, P., Kannenberg, F., Fobker, M., Engel, T., Denis, S., Wouters, F., Wirtz, K. W., Wanders, R. J., Maeda, N., and Assmann, G. (1998) Defective peroxisomal catabolism of branched fatty acyl coenzyme A in mice lacking the sterol carrier protein-2/sterol carrier protein-x gene function, *Genes Dev. 12*, 1189−1201.
7. Russell, D. W. (2003) The enzymes, regulation, and genetics of bile acid synthesis, *Annu. Rev. Biochem. 72*, 137−174.
8. Wanders, R. J., Vreken, P., Ferdinandusse, S., Jansen, G. A., Waterham, H. R., van Roermund, C. W., and Van Grunsven, E. G. (2001) Peroxisomal fatty acid alpha- and beta-oxidation in humans: enzymology, peroxisomal metabolite transporters and peroxisomal diseases, *Biochem. Soc. Trans. 29*, 250−267.
9. Seedorf, U., Ellinghaus, P., and Roch, Nofer, J. (2000) Sterol carrier protein-2, *Biochim. Biophys. Acta 1486*, 45−54.
10. Haapalainen, A. M., van Aalten, D. M., Merilainen, G., Jalonen, J. E., Pirila, P., Wierenga, R. K., Hiltunen, J. K., and Glumoff, T. (2001) Crystal structure of the liganded SCP-2-like domain of human peroxisomal multifunctional enzyme type 2 at 1.75 Å resolution, *J. Mol. Biol. 313*, 1127−1138.
11. Dyer, D. H., Lovell, S., Thoden, J. B., Holden, H. M., Rayment, I., and Lan, Q. (2003) The structural determination of an insect sterol carrier protein-2 with a ligand-bound C16 fatty acid at 1.35-Å resolution, *J. Biol. Chem. 278*, 39085−39091.
12. Garcia, F. L., Szyperski, T., Dyer, J. H., Choinowski, T., Seedorf, U., Hauser, H., and Wuthrich, K. (2000) NMR structure of the sterol carrier protein-2: implications for the biological role, *J. Mol. Biol. 295*, 595−603.
13. Choinowski, T., Hauser, H., and Piontek, K. (2000) Structure of sterol carrier protein 2 at 1.8 Å resolution reveals a hydrophobic tunnel suitable for lipid binding, *Biochemistry 39*, 1897−1902.
14. Weber, F. E., Dyer, J. H., Garcia, F. L., Werder, M., Szyperski, T., and Wuthrich, K. (1998) In pre-sterol carrier protein 2 (SCP2) in solution the leader peptide is flexibly disordered, and residues 21−143 adopt the same globular fold as in mature SCP2), *Cell. Mol. Life Sci. 54*, 751−759.
15. Gatto, G. J., Jr., Geisbrecht, B. V., Gould, S. J., and Berg, J. M. (2000) Peroxisomal targeting signal-1 recognition by the TPR domains of human PEX5, *Nat. Struct. Biol. 7*, 1091−1095.
16. Heiland, I., and Erdmann, R. (2005) Biogenesis of peroxisomes. Topogenesis of the peroxisomal membrane and matrix proteins, *FEBS J. 272*, 2362−2372.
17. Lensink, M. F., Haapalainen, A. M., Hiltunen, J. K., Glumoff, T., and Juffer, A. H. (2002) Response of SCP-2L domain of human MFE-2 to ligand removal: binding site closure and burial of peroxisomal targeting signal, *J. Mol. Biol. 323*, 99−113.
18. Schroeder, F., Frolov, A., Starodub, O., Atshaves, B. B., Russell, W., Petrescu, A., Huang, H., Gallegos, A. M., McIntosh, A., Tahotna, D., Russell, D. H., Billheimer, J. T., Baum, C. L., and Kier, A. B. (2000) Pro-sterol carrier protein-2: role of the N-terminal presequence in structure, function, and peroxisomal targeting, *J. Biol. Chem. 275*, 25547−25555.
19. Stolowich, N. J., Petrescu, A. D., Huang, H., Martin, G. G., Scott, A. I., and Schroeder, F. (2002) Sterol carrier protein-2: structure reveals function, *Cell. Mol. Life Sci. 59*, 193−212.
20. Stanley, W. A., Sokolova, A., Brown, A., Clarke, D. T., Wilmanns, M., and Svergun, D. I. (2004) Synergistic use of synchrotron radiation techniques for biological samples in solution: a case study on protein-ligand recognition by the peroxisomal import receptor Pex5p, *J. Synchrotron Radiat. 11*, 490−496.
21. Sattler, M., Schleucher, J. and Griesinger, C. (1999) Heteronuclear multidimensional NMR experiments for the structure determination of proteins in solution employing pulsed field gradients, *Prog. NMR Spectrosc. 34*, 93−158.
22. Reis, S., Moutinho, C. G., Matos, C., de Castro, B., Gameiro, P., and Lima, J. L. (2004) Noninvasive methods to determine the critical micelle concentration of some bile acid salts, *Anal. Biochem. 334*, 117−126.
23. Powell, G. L., Grothusen, J. R., Zimmerman, J. K., Evans, C. A., and Fish, W. W. (1981) A re-examination of some properties of fatty acyl-CoA micelles, *J. Biol. Chem. 256*, 12740−12747.
24. Farrow, N. A., Muhandiram, R., Singer, A. U., Pascal, S. M., Kay, C. M., Gish, G., Shoelson, S. E., Pawson, T., Forman-Kay, J. D., and Kay, L. E. (1994) Backbone dynamics of a free and phosphopeptide-complexed Src homology 2 domain studied by ^{15}N NMR relaxation, *Biochemistry 33*, 5984−6003.
25. Mulder, F. A., Spronk, C. A., Slijper, M., Kaptein, R., and Boelens, R. (1996) Improved HSQC experiments for the observation of exchange broadened signals, *J. Biomol. NMR 8*, 223−228.
26. Stanley, W. A., Filipp, F. V., Kursula, P., Erdmann, R., Schliebs, W., Sattler, M., and Wilmanns, M. (2006) Recognition of a functional peroxisome type 1 target by the dynamic import receptor Pex5p, *Mol. Cell 24*, 653−663.
27. Battiste, J. L., and Wagner, G. (2000) Utilization of site-directed spin labeling and high-resolution heteronuclear nuclear magnetic resonance for global fold determination of large proteins with limited nuclear overhauser effect data, *Biochemistry 39*, 5355−5365.
28. Stolowich, N., Frolov, A., Petrescu, A. D., Scott, A. I., Billheimer, J. T., and Schroeder, F. (1999) Holo-sterol carrier protein-2. (13)C NMR investigation of cholesterol and fatty acid binding sites, *J. Biol. Chem. 274*, 35425−35433.
29. Huyghues-Despointes, B. M., Pace, C. N., Englander, S. W., and Scholtz, J. M. (2001) Measuring the conformational stability of a protein by hydrogen exchange, *Methods Mol. Biol. 168*, 69−92.

30. Baxter, N. J., Hosszu, L. L., Waltho, J. P., and Williamson, M. P. (1998) Characterisation of low free-energy excited states of folded proteins, *J. Mol. Biol. 284*, 1625−1639.
31. Mulder, F. A., van Tilborg, P. J., Kaptein, R., and Boelens, R. (1999) Microsecond time scale dynamics in the RXR DNA-binding domain from a combination of spin-echo and off-resonance rotating frame relaxation measurements, *J. Biomol. NMR 13*, 275−288.
32. Palmer, A. G., III, Grey, M. J., and Wang, C. (2005) Solution NMR spin relaxation methods for characterizing chemical exchange in high-molecular-weight systems, *Methods Enzymol. 394*, 430−465.
33. Mueller, L., Legault, P., and Pardi, A. (1995) Improved RNA structure determination by detection of NOE contacts to exchange-broadened amino protons, *J. Am. Chem. Soc. 117*, 11043−11048.
34. McNew, J. A., and Goodman, J. M. (1996) The targeting and assembly of peroxisomal proteins: some old rules do not apply, *Trends Biochem. Sci. 21*, 54−58.
35. Schroeder, F., Myers-Payne, S. C., Billheimer, J. T., and Wood, W. G. (1995) Probing the ligand binding sites of fatty acid and sterol carrier proteins: effects of ethanol, *Biochemistry 34*, 11919−11927.
36. Mulder, F. A., Skrynnikov, N. R., Hon, B., Dahlquist, F. W., and Kay, L. E. (2001) Measurement of slow (μs-ms) time scale dynamics in protein side chains by (15)N relaxation dispersion NMR spectroscopy: application to Asn and Gln residues in a cavity mutant of T4 lysozyme, *J. Am. Chem. Soc. 123*, 967−975.
37. Nichesola, D., Perduca, M., Capaldi, S., Carrizo, M. E., Righetti, P. G., and Monaco, H. L. (2004) Crystal structure of chicken liver basic fatty acid-binding protein complexed with cholic acid, *Biochemistry 43*, 14072−14079.
38. Constantine, K. L., Friedrichs, M. S., Wittekind, M., Jamil, H., Chu, C. H., Parker, R. A., Goldfarb, V., Mueller, L., and Farmer, B. T., II (1998) Backbone and side chain dynamics of uncomplexed human adipocyte and muscle fatty acid-binding proteins, *Biochemistry 37*, 7965−7980.
39. Zhu, L., Kurian, E., Prendergast, F. G., and Kemple, M. D. (1999) Dynamics of palmitic acid complexed with rat intestinal fatty acid binding protein, *Biochemistry 38*, 1554−1561.
40. Hamilton, J. A., Cistola, D. P., Morrisett, J. D., Sparrow, J. T., and Small, D. M. (1984) Interactions of myristic acid with bovine serum albumin: a ^{13}C NMR study, *Proc. Natl. Acad. Sci. U.S.A. 81*, 3718−3722.

BI6025616